Optics Letters

Flexible waveguide integrated thermo-optic switch based on TiO_2 platform

Zequn Chen,[1,2,3] Maoliang Wei,[4,5] Boshu Sun,[2,3] Yang Weng,[2,3] Jialing Jian,[2,3] Chuyu Zhong,[4,5] Chunlei Sun,[2,3] Ke Si,[4] Wei Gong,[4] Hongtao Lin,[4,5] and Lan Li[2,3,*]

[1]Zhejiang University, Hangzhou 310027, China
[2]Key Laboratory of 3D Micro/Nano Fabrication and Characterization of Zhejiang Province, School of Engineering, Westlake University, Hangzhou 310024, China
[3]Institute of Advanced Technology, Westlake Institute for Advanced Study, Hangzhou 310024, China
[4]MOE Frontier Science Center for Brain Science & Brain–Machine Integration, Zhejiang University, Hangzhou 310027, China
[5]State Key Laboratory of Modern Optical Instrumentation, College of Information Science and Electronic Engineer, Zhejiang University, Hangzhou 310027, China
*lilan@westlake.edu.cn

Received 22 December 2022; revised 30 April 2023; accepted 7 May 2023; posted 8 May 2023; published 12 June 2023

Mechanically flexible photonic devices are critical components of novel bio-integrated optoelectronic and high-end wearable systems, in which thermo-optic switches (TOSs) as optical signal control devices are crucial. In this paper, flexible titanium oxide (TiO_2) TOSs based on a Mach–Zehnder interferometer (MZI) structure were demonstrated around 1310 nm for, it is believed, the first time. The insertion loss of flexible passive TiO_2 2×2 multi-mode interferometers (MMIs) is −3.1 dB per MMI. The demonstrated flexible TOS achieves power consumption (P_π) of 0.83 mW, compared with its rigid counterpart, for which P_π is decreased by a factor of 18. The proposed device could withstand 100 consecutive bending operations without noticeable degradation in TOS performance, indicating excellent mechanical stability. These results provide a new perspective for designing and fabricating flexible TOSs for flexible optoelectronic systems in future emerging applications.

https://doi.org/10.1364/OL.484113

Compared with traditional optoelectronics, flexible optoelectronic devices are more adaptable to various working environments. Emerging applications of mechanically flexible photonic systems have blossomed in such fields as optical interconnects [1,2], strain sensing [3,4], temperature sensing [5], implantable optogenetic probes [6,7], brain–computer interfaces [8], and optical tuning [9]. Flexible thermo-optic switches (TOSs) are a basic component of such systems and have received great attention and research efforts in academia and the industry. For a flexible TOS design to succeed, high-density integration capability and superior mechanical robustness and optical properties, such as low power consumption and low insertion loss, are necessary to meet the requirements of the aforementioned applications.

At present, TOSs have been successfully produced on many material platforms, including silicon (Si) [10,11], silicon nitride (SiN) [12], lithium niobate [13], chalcogenide glass [14], and polymer [15–17]. However, in research on flexible TOSs, few material platforms can simultaneously satisfy the aforementioned requirements. For instance, owing to their natural flexibility, large negative thermo-optic coefficient (TOC), and ease of machining [16], polymers are the preferred choice for fabricating flexible TOSs with low power consumption. However, the relatively low refractive index and poor electronic and thermal properties of polymers limit their potential for high-density integration and long-term device stability. In addition, though a high-index-contrast (HIC) structure can be achieved by combining inorganic materials, such as Si or SiN, with a polymer substrate, it is very complicated to prepare flexible waveguide integrated devices [18,19] because these materials cannot be directly deposited on the flexible substrate. Amorphous silicon [20] and chalcogenide glass [21] can be deposited directly on polymer substrates at a lower temperature. However, the TOC of the silicon-based materials and chalcogenide glass is positive, which is opposite to the negative TOC of the flexible substrate, leading to a decrease in thermal modulation performance, fundamentally limiting the application of most optical materials in the development of flexible TOS devices. Therefore, it is necessary to develop a material that has a high refractive index, is easy to process, and holds a large negative TOC consistent with polymer substrates to realize compact TOSs with low power consumption.

Titanium oxide (TiO_2) has a large negative TOC (−0.5 to $-2.4\times10^{-4}\,K^{-1}$) and can be prepared near room temperature [22,23], which means that it can be directly deposited on most substrates. Both TiO_2 and the polymer have a negative TOC, and the synergistic effect of two negative TOC materials can further enhance the thermo-optic (TO) modulation performance [23]. Moreover, the high refractive index ($n=2.32$ @ 1310 nm) of TiO_2 combined with the flexible substrate to form the HIC structure provides strong optical confinement and additional freedom in the design and optimization of the modulation and routing of multi-channel signals [24–26]. However, there are only a few reports on thermal-insensitive silicon-based modulators using TiO_2 as the top cladding [27,28] and the TiO_2 waveguide TO

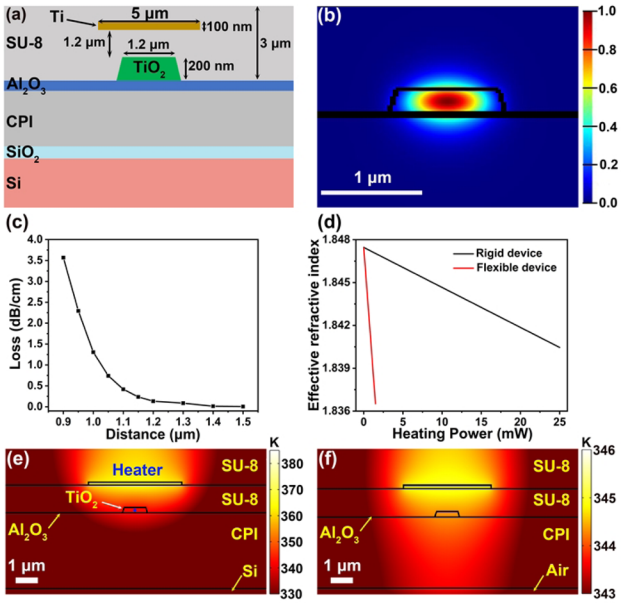

Fig. 1. (a) Cross section of TiO_2 waveguide with microheater. (b) Fundamental TE mode of TiO_2 waveguide at 1310 nm. (c) Simulated waveguide propagation loss as a function of the gap between the waveguide and the heater. (d) Effective refractive index of TiO_2 waveguide versus heating power. (e), (f) Calculated temperature distribution at individual heating power of P_π: (e) rigid device (12 mW); (f) flexible device (0.45 mW).

modulation [23,29]; research on flexible TiO_2 TOSs is rarely reported.

In this work, we first demonstrated a simple strategy to implement flexible TOSs based on the Mach–Zehnder interferometer (MZI) structure using magnetron-sputtering TiO_2. As a result, the insertion loss of the proposed flexible passive TiO_2 2×2 platforms with multi-mode interferometers (MMIs) is −3.1 dB per MMI, which satisfies the requirement of a low insertion loss for flexible TOSs. Because both the polymer substrate and TiO_2 have a negative TOC, the π phase-shift power consumption (P_π) of the rigid TOSs (before peeling to give flexible TOSs) is 15.1 mW, which is even smaller than that of some SiN [12] and Si TOSs [30]. Taken together with the advantages of the HIC structure, the size of TiO_2 TOSs is two orders of magnitude smaller than that of the polymer TOSs. Furthermore, removing the silicon substrate beneath the TiO_2 TOSs makes the device flexible, with the corresponding P_π being 0.83 mW, 18 times lower than that of rigid TOSs. After 100 bending cycles, flexible TiO_2 TOSs showed no obvious attenuation in device optical performance, proving the excellent mechanical stability of the device. This method demonstrates a new perspective on the design and fabrication of efficient flexible TOSs and can also be applied to a broad range of flexible optoelectronic devices, such as implantable probes, integrated modulators, and on-chip light sources, and finally realize fully integrated flexible photonic integrated circuits.

We first carried out TO simulation of TOS devices by finite-element modeling (FEM) analysis. The device cross section is shown schematically in Fig. 1(a). The TiO_2 waveguide is a ridge waveguide with 1.2 μm width and a sidewall angle of 67° [23], supporting the fundamental TE mode [Fig. 1(b)]. The heater thickness and width are 100 nm and 5 μm, respectively. In addition, the spacing between the heater and the waveguide was optimized and chosen as 1.2 μm to minimize the loss caused by the heater and ensure heating efficiency at the same time [Fig. 1(c)]. When a voltage is applied to the heater, the temperature of the waveguide will be altered by joule heating. With a negative TOC in TiO_2 material, the phase tuning $\Delta\varphi$ of the waveguide is proportional to the temperature change ΔT, being expressed as [23]

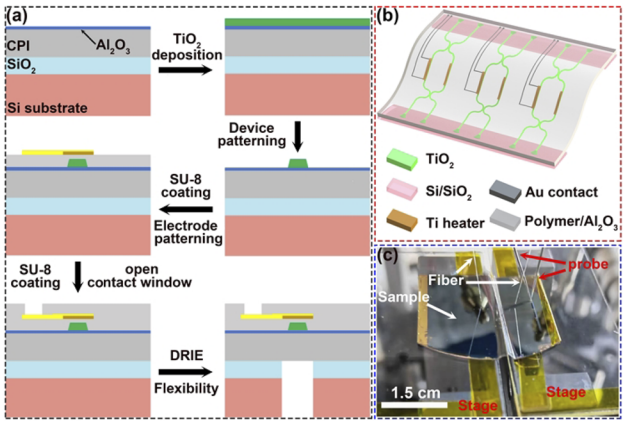

Fig. 2. (a) TiO_2 device preparation process. (b) Flexible TiO_2 TOSs based on MZI. (c) Flexible TiO_2 passive or active devices under test.

$$\Delta\varphi = \frac{2\pi L}{\lambda_0}\left(\frac{\mathrm{d}n}{\mathrm{d}T}\right)\Delta T, \tag{1}$$

where λ_0 is the working wavelength, L is the heater length, and $\mathrm{d}n/\mathrm{d}T$ is the TOC of TiO_2. Figure 1(d) shows the simulation results of the effective refractive index of the TiO_2 waveguide versus the heating power. When the effective refractive index of TiO_2 changes by 0.0033, the theoretically calculated P_π of the TOS on the rigid substrate is 12 mW. Conversely, when the rigid substrate at the bottom of the device is removed, the device becomes free-standing and flexible, and the air acts as a poor thermal conductive medium between the device and the environment, resulting in better heat accumulation. Figures 1(e) and 1(f) show the temperature distribution of the devices at individual heating power P_π. In flexible TOSs, the heat energy is much more localized within the device; thus, only a P_π of 0.45 mW is required to achieve π phase change.

The preparation process following the optimization of the device is shown in Fig. 2(a). First, on the bare silicon, 300 nm silicon oxide (SiO_2; plasma-enhanced chemical vapor deposition, PECVD), colorless polyimide (CPI; spin-coating, 2000 rpm, 1 min, followed by 80°C for 30 min, 150°C for 30 min, 200°C for 30 min, 280°C for 30 min in sequence in a vacuum oven), and 30 nm alumina (Al_2O_3; atomic layer deposition, ALD) were successively deposited. 200 nm TiO_2 thin film was then deposited on Al_2O_3 by reactive sputtering (400 W). The 30 nm Al_2O_3 can shield the CPI from bombardment by oxygen plasma during the sputtering process [31]. After the electron beam lithography (EBL) (Raith Voyager, 30 kV) and inductively coupled plasma reactive ion etching (ICP-RIE) process, the device pattern was transferred onto TiO_2. A layer of SU-8 with a thickness of 1.2 μm was then deposited on the TiO_2 device to produce the passive device. For TOS fabrication, heater electrodes (100 nm

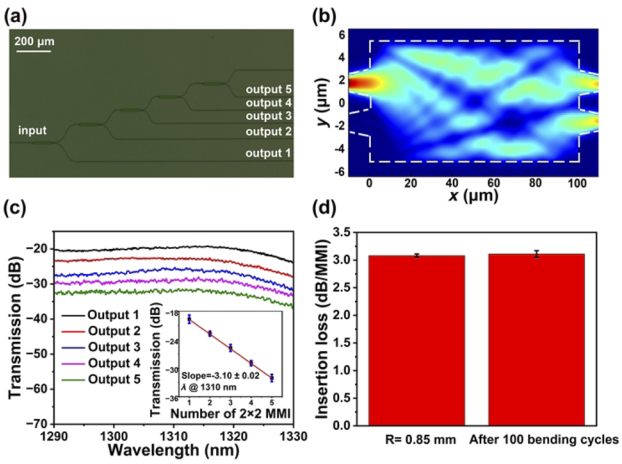

Fig. 3. (a) Micrograph of TiO_2 device based on cascade of 2×2 MMIs. (b) Simulated electric field distribution of optimized TiO_2 2×2 MMI. (c) Insertion loss measurements of flexible TiO_2 2×2 MMI at bending radius $R=\infty$. Inset: Measured transmission of cascaded TiO_2 2×2 MMI tree as a function of number of 2×2 MMIs. (d) Insertion loss measurements of flexible TiO_2 2×2 MMI at bending radii $R=0.85$ mm and $R=\infty$ after 100 bendings.

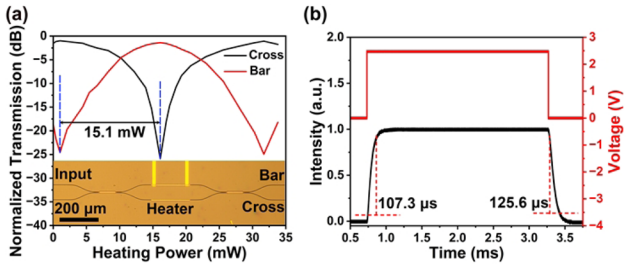

Fig. 4. (a) Normalized transmission of cross and bar ports of rigid TOS at 1310 nm under different applied heating powers. Insert: micrograph of TOS. (b) Time response of MZI-based TiO_2 TOS on silicon.

Ti/5 nm Au) and contact pads (5 nm Ti/100 nm Au) were patterned using lithography and deposited by e-beam evaporation on the as-prepared devices, followed by another 1.8 μm SU-8 coating and opening of the pad window for probe contact via lithography. The total thickness of SU-8 is about 3 μm, balanced with the CPI thickness (3 μm) to allow the TiO_2 structures to be located at the neutral axis, achieving an almost stress-free effect on TiO_2 when the device is bending [21]. To prepare flexible TOSs, we performed deep reactive ion etching (DRIE) on the backside of the device, and the SiO_2 serves as the reaction stop layer. Finally, the SiO_2 was corroded with diluted HF (HF: deionized water, 1: 20), so the local working device became free-standing and flexible. Figure 2(b) is a three-dimensional (3D) schematic of the MZI–MMI flexible TOS. As opposed to a completely free-standing device, this method not only realizes the flexibility of the device, but also greatly facilitates the testing of the flexible active waveguide integrated devices [32], as shown in Fig. 2(c). The device was coupled to the input and output fibers by focusing grating couplers inclined by 8° to achieve efficient coupling, where the optical transmission spectrum was collected using a broadband tunable laser system (Santec full-band TSL-550). For the flexible device test, the bending of the device was controlled by the spacing between movable stages below the chip. For the static thermally tuned measurements, a voltage was applied using a source meter to heat the waveguide. A power meter was used to read the emitted optical signal. The modulation voltage was applied to an arbitrary waveform generator (AWG, Siglent SDG6032X-E) for the purpose of dynamic characterization. A photodetector was attached to the optical output of the device. An oscilloscope (Siglent SDS5104X) was used to record the modulation signals and obtain the device response time.

As an integral component of flexible TOSs, the flexible passive TiO_2 2×2 MMI was first fabricated and characterized. A cascade of a 2×2 MMI device is shown in Fig. 3(a). The length and width of the design-optimized TiO_2 2×2 MMI region are 100.3 μm and 10.2 μm, respectively. The width of the waveguide is 1.2 μm. The taper length is 10 μm. Figure 3(b) shows the simulated electric field distribution of the mode profile for the optimized 2×2 MMI, indicating low cross talk at the input and uniform power splitting at the output. As shown in Fig. 3(c), at the bending radius $R=\infty$, the insertion loss of a TiO_2 2×2 MMI is approximately −3.1 dB per MMI measured from input to outputs 1–5 [Fig. 3(a)]. We also carried out mechanical fatigue tests [Fig. 3(d)]. The device under a bending radius of 0.85 mm indicates an insertion loss of -3.08 ± 0.03 dB per MMI. We repeatedly folded the flexible 2×2 MMI device from $R=\infty$ to $R=0.85$ mm, and the insertion loss was -3.11 ± 0.06 dB per MMI after 100 bending cycles, demonstrating robust mechanical and optical performance.

Before verifying the performance of flexible TOSs, we first characterized their rigid counterparts. Figure 4(a) shows the normalized transmission of the bar and cross ports at 1310 nm under different heating powers on one arm. The switch indicates a cross talk of −24.5 dB, an extinction ratio of 24.9 dB and an insertion loss of ∼1 dB. Under a bias of 2.5 V, the device achieves π phase shift and consumes a power of 15.1 mW. (The simulated P_π is 12 mW). We further characterized the dynamic response of the sputtering TiO_2 2×2 MMI TOSs. As shown in Fig. 4(b), the rise and fall times measured at 2.5 V are 107.3 μs and 125.6 μs, respectively, which could meet the requirements of such applications as upconversion optogenetics [33] for a sub-millisecond response and on-chip spectrometer [34]. Meanwhile, the P_π of 15.1 mW is much less than the power consumption of some Si [30] or SiN TOSs [12], illustrating the synergistic effect between TiO_2 and polymer substrates with negative TOC. Compared with TOSs based on polymer waveguides, our device is two orders of magnitude smaller than polymer devices [16], showing an advantage of the HIC platform.

Furthermore, to achieve flexible TOSs, the rigid substrate at the bottom of the TOSs was removed by DRIE. The entire TOS is free-standing; thus, air is the contact medium between the device and the environment. Since the thermal conductivity of air is much lower than that of silicon wafers, it can be seen in Fig. 5(a) that, for a bending radius of $R=\infty$, under a bias voltage of 0.65 V, the cross talk of the flexible TiO_2 TOS is −22.5 dB and P_π is only 0.83 mW. A possible cause for the deviation between the experimentally measured P_π of 0.83 mW and the corresponding simulation result of 0.45 mW could be differences between the simulated material parameters and the actual material parameters, as well as the potential omission of testing and coupling factors in the simulation. The corresponding rise and fall times are 1.15 ms and 1.62 ms, respectively [Fig. 5(b)].

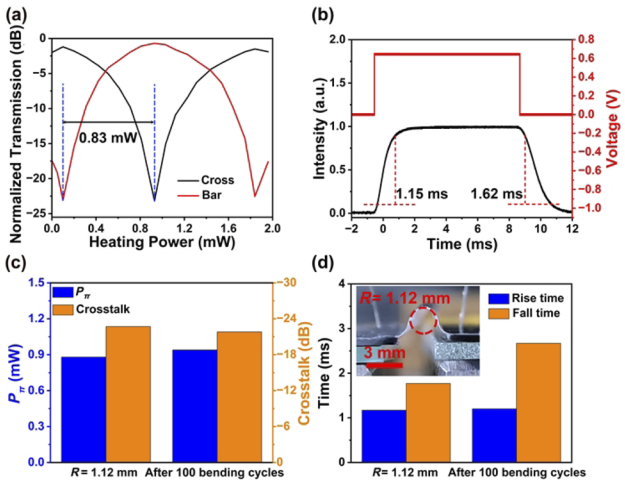

Fig. 5. (a) Normalized transmission of cross and bar ports of flexible TOS at 1310 nm as a function of applied heating power. (b) Time response of MZI-based flexible TiO_2 TOS. (c), (d) Analysis of device at bending radii $R = 1.12$ mm and $R = \infty$ after 100 bends: (c) P_π and cross talk; (d) rise and fall times. Inset of (d): Cross section of device.

We also tested the TOS performance of the device at bending radii of $R = 1.12$ mm and $R = \infty$ after 100 times of bending from $R = \infty$ to $R = 1.12$ mm. The P_π of the device is 0.88 mW and 0.94 mW, the cross talk is −22.7 dB and −21.8 dB, and the response times are 1.77 ms and 2.67 ms, respectively, as shown in Figs. 5(c) and 5(d). The device's optical performance is stable on bending, proving the mechanical robustness of the device. To date, the P_π of 0.83 mW is the lowest among flexible TOSs, to our knowledge, and the flexible TiO_2 TOS is also two orders of magnitude smaller than polymer-based TOSs [16]. Although the response time is in milliseconds, it can still be implemented in wearable devices to treat neurological diseases, such as for hearing recovery [35].

In conclusion, we have successfully prepared flexible TiO_2 TOSs with low power consumption. The insertion loss of the passive flexible 2×2 MMI is 0.1 dB. The resulting flexible TOS exhibits a P_π of 0.83 mW, which is 18 times lower than the rigid TOS, mainly attributed to the poor thermal conductivity of the air. In addition, the device still shows comparable performance to the original device after 100 consecutive bendings. Our schemes provide a new route for developing and preparing flexible TOSs and pave the way for many applications, including conformal sensing, implantable devices, and optical communication.

Funding. National Natural Science Foundation of China (62175202, 12104375); Natural Science Foundation of Zhejiang Province (LD22F040002); Leading Innovative and Entrepreneur Team Introduction Program of Zhejiang (2020R01005); MOE Frontier Science Center for Brain Science & Brain-Machine Integration, Zhejiang University.

Acknowledgments. We acknowledge Westlake Center for Micro/Nano Fabrication at Westlake University for facility support. We also thank Yating Pan for her help in the metal deposition.

Disclosures. The authors declare no conflicts of interest.

Data availability. Data underlying the results presented in this paper are not publicly available at this time but may be obtained from the authors upon reasonable request.

REFERENCES

1. L. Li, Y. Zou, H. Lin, J. Hu, X. Sun, N. N. Feng, S. Danto, K. Richardson, T. Gu, and M. Haney, J. Lightwave Technol. **31**, 4080 (2013).
2. R. B. Tipton, D. Hou, Z. Shi, T. M. Weller, and V. R. Bhethanabotla, Addit. Manuf. **48**, 102409 (2021).
3. S. Yun, S. Park, B. Park, Y. Kim, S. K. Park, S. Nam, and K.-U. Kyung, Adv. Mater. **26**, 4474 (2014).
4. C. Zhang, H. Dong, C. Zhang, Y. Fan, J. Yao, and Y. S. Zhao, Sci. Adv. **7**, eabh3530 (2021).
5. L. Gao, Y. Zhang, V. Malyarchuk, L. Jia, K.-I. Jang, R. Chad Webb, H. Fu, Y. Shi, G. Zhou, L. Shi, D. Shah, X. Huang, B. Xu, C. Yu, Y. Huang, and J. A. Rogers, Nat. Commun. **5**, 4938 (2014).
6. T. Pan, D. Lu, H. Xin, and B. Li, Light: Sci. Appl. **10**, 124 (2021).
7. W. Bai, J. Shin, and R. Fu, *et al.*, Nat. Biomed. Eng. **3**, 644 (2019).
8. Z. Chen and L. Li, Acc. Mater. Res. **2**, 315 (2021).
9. S. Nam, D. Wang, G. Lee, and S. S. Choi, Nanophotonics **11**, 2139 (2022).
10. F. Duan, K. Chen, D. Chen, and Y. Yu, Opt. Lett. **46**, 234 (2021).
11. G. Zhang, J. Y. Haw, H. Cai, F. Xu, S. M. Assad, J. F. Fitzsimons, X. Zhou, Y. Zhang, S. Yu, J. Wu, W. Ser, L. C. Kwek, and A. Q. Liu, Nat. Photonics **13**, 839 (2019).
12. A. Mohanty, Q. Li, M. A. Tadayon, S. P. Roberts, G. R. Bhatt, E. Shim, X. Ji, J. Cardenas, S. A. Miller, A. Kepecs, and M. Lipson, Nat. Biomed. Eng. **4**, 223 (2020).
13. X. Liu, P. Ying, X. Zhong, J. Xu, Y. Han, S. Yu, and X. Cai, Opt. Lett. **45**, 6318 (2020).
14. H. Lin, Y. Song, and Y. Huang, *et al.*, Nat. Photonics **11**, 798 (2017).
15. B. Lin, X. Wang, J. Lv, Y. Cao, Y. Yang, Y. Zhang, A. Zhang, Y. Yi, F. Wang, and D. Zhang, Opt. Lett. **45**, 4448 (2020).
16. Y. Sun, Y. Cao, Q. Wang, Y. Yi, X. Sun, Y. Wu, F. Wang, and D. Zhang, Appl. Opt. **57**, 14 (2018).
17. X. Wang, W. Jin, Z. Chang, and K. S. Chiang, Opt. Lett. **44**, 1480 (2019).
18. Y. Chen and M. Li, Opt. Lett. **39**, 3449 (2014).
19. Y. Chen, H. Li, and M. Li, Sci. Rep. **2**, 622 (2012).
20. L. Fan, L. T. Varghese, Y. Xuan, J. Wang, B. Niu, and M. Qi, Opt. Express **20**, 20564 (2012).
21. L. Li, H. Lin, S. Qiao, Y. Zou, S. Danto, K. Richardson, J. D. Musgraves, N. Lu, and J. Hu, Nat. Photonics **8**, 643 (2014).
22. H. Park, J. Jung, Y. Zhang, M. Liu, J. Lee, H. Noh, M. Choi, S. Lee, and H. Park, ACS Appl. Electron. Mater. **4**, 651 (2022).
23. Z. Chen, M. Wei, Y. Luo, J. Jian, Y. Ye, Y. Yin, C. Sun, C. Zhong, K. Si, D. Zhang, H. Lin, and L. Li, Opt. Mater. Express **12**, 4061 (2022).
24. Y.-B. Kim, J.-W. Cho, Y.-J. Lee, D. Bae, and S.-K. Kim, Light: Sci. Appl. **11**, 316 (2022).
25. A. Melloni, R. Costa, G. Cusmai, and F. Morichetti, Int. J. Mater. Prod. Technol. **34**, 421 (2009).
26. J. T. Robinson, K. Preston, O. Painter, and M. Lipson, Opt. Express **16**, 16659 (2008).
27. B. Guha, J. Cardenas, and M. Lipson, Opt. Express **21**, 26557 (2013).
28. S. S. Djordjevic, K. Shang, B. Guan, S. T. S. Cheung, L. Liao, J. Basak, H.-F. Liu, and S. J. B. Yoo, Opt. Express **21**, 13958 (2013).
29. H. Yu and F. Qiu, Opt. Lett. **47**, 2093 (2022).
30. W. Shen, J. Du, K. Xu, and Z. He, IEEE Photonics Technol. Lett. **33**, 483 (2021).
31. L. Li, P. Zhang, W.-M. Wang, H. Lin, A. B. Zerdoum, S. J. Geiger, Y. Liu, N. Xiao, Y. Zou, O. Ogbuu, Q. Du, X. Jia, J. Li, and J. Hu, Sci. Rep. **5**, 13832 (2015).
32. L. Li, H. Lin, Y. Huang, R.-J. Shiue, A. Yadav, J. Li, J. Michon, D. Englund, K. Richardson, T. Gu, and J. Hu, Optica **5**, 44 (2018).
33. S. Chen, A. Z. Weitemier, X. Zeng, L. He, X. Wang, Y. Tao, A. J. Y. Huang, Y. Hashimotodani, M. Kano, H. Iwasaki, L. K. Parajuli, S. Okabe, D. B. L. Teh, A. H. All, I. Tsutsui-Kimura, K. F. Tanaka, X. Liu, and T. J. McHugh, Science **359**, 679 (2018).
34. C. Sun, Y. Yin, Z. Chen, Y. Ye, Y. Luo, H. Ma, L. Wang, M. Wei, J. Jian, R. Tang, H. Dai, J. Wu, J. Li, D. Zhang, H. Lin, and L. Li, PhotoniX **3**, 12 (2022).
35. T. Michael, K. Lexie, S. Sarah, K. Komal, T. Xiaodong, H. Razi-ul, and R. Claus-Peter, Proc.SPIE **11935**, 1193502 (2022).